ETH-TH/97-6 DTP/97/08 hep-ph/9702286 January 1997

Diffractive Higgs Production at the LHC

M. Heyssler

Department of Physics, University of Durham Durham DH1 3LE, England

Z. Kunszt

Institute of Theoretical Physics, ETH CH-8093 Zurich, Switzerland

and

W.J. Stirling

Departments of Mathematical Sciences and Physics, University of Durham Durham DH1 3LE, England

Abstract

We use diffractive parton distributions obtained from fits to the diffractive structure function measured at HERA to predict cross sections for single diffractive Higgs production at the LHC. The dominant background processes are also considered. Although some 5% - 15% of Higgs events are predicted to be diffractive in this model, the ratio of signal to background is not significantly improved. The fact that a significant fraction of deep inelastic scattering events seen at the HERA *ep* collider have a diffractive ('rapidity gap') structure has led to suggestions that 'hard diffractive scattering' may be a relatively common occurrence at high–energy lepton–hadron and hadron–hadron colliders and, furthermore, that such diffractive topologies may help to enhance certain new physics signals over backgrounds. In this letter we wish to explore further the idea [1, 2] that single diffractive production may be a useful additional tool for identifying the Higgs boson at the LHC.

An important property of the HERA diffractive deep inelastic scattering events [3] is the approximate factorization of the structure function F_2^D (integrated over t) into a function of $x_{\mathcal{P}}$ times a function of $\xi = x_{\mathrm{Bj}}/x_{\mathcal{P}}$: $F_2^D \sim x_{\mathcal{P}}^{-n}\mathcal{F}(\xi,Q^2)$. This property, together with the observed rapidity–gap topology of the events, strongly suggests that the deep inelastic scattering takes place off a slow–moving colourless target \mathcal{P} 'emitted' by the proton, $p \to \mathcal{P}p$, and with a fraction $x_{\mathcal{P}} \ll 1$ of its momentum. If this emission is described by a universal flux function $f_{\mathcal{P}}(x_{\mathcal{P}}, t)dx_{\mathcal{P}}dt$, then the diffractive structure function F_2^D is simply a product of this and the structure function of the colourless object, $F_2^{\mathcal{P}}(\xi, Q^2)$. Since the scattering evidently takes place off point–like charged objects, we may write the latter as a sum over quark–parton distributions, i.e. $F_2^{\mathcal{P}}(\xi, Q^2) = \xi \sum_q e_q^2 q_{\mathcal{P}}(\xi, Q^2)$, in leading order. In this way we obtain a model for the diffractive parton distributions:

$$\frac{df_{q/p}(x,\mu^2;x_{\mathcal{P}},t)}{dx_{\mathcal{P}}dt} = f_{\mathcal{P}}(x_{\mathcal{P}},t) f_{q/\mathcal{P}}(\xi = x/x_{\mathcal{P}},\mu^2) .$$
(1)

If one assumes further that the colour-neutral target is the Regge pomeron, then the emission factor $f_{\mathcal{P}}$ is already known from soft hadronic physics (for a review see Ref. [4]): $f_{\mathbb{P}}(x^{\mathbb{P}},t) = F_{\mathbb{P}}(t)(x^{\mathbb{P}})^{2\alpha_{\mathbb{P}}(t)-1}$, which gives a factorized structure function with $n \approx 2\alpha_{\mathbb{P}}(0) - 1 \approx 1.16$. This model is based on the notion of 'parton constituents in the pomeron' first proposed by Ingelman and Schlein [5] and supported by data from UA8 [6]. In such a model, a modest amount of factorization breaking, such as that observed in the more recent H1 and ZEUS analyses [7, 8], could be accommodated by invoking a sum over Regge trajectories, each with a different intercept and structure function, see for example Ref. [9]. In the present study we assume, for simplicity, pomeron exchange only and use the parametrization of Ref. [10] for $\alpha_{\mathbb{P}}(t)$ and $F_{\mathbb{P}}(t)$. The $x^{\mathbb{P}}$ dependence of the diffractive structure function predicted by this type of 'soft pomeron' model is roughly consistent within errors with the H1 [7] and ZEUS [8] data, although there is some indication that a somewhat steeper $x^{\mathbb{P}}$ dependence is preferred.

Although the above picture of deep inelastic scattering taking place off hard parton constituents in a 'soft' pomeron gives a good description of the HERA data, the generalization to other hard scattering processes, and in particular the concept of 'universal pomeron structure' is on a much less firmer theoretical footing, see for example Ref. [11]. One of the cleanest processes to test this hypothesis would appear to be diffractive W^{\pm} and Z^0 production at the Tevatron, i.e. $p\bar{p}$ collisions at $\sqrt{s} = 1.8$ TeV [12, 13]. According to Ref. [13], some 7% of W events should exhibit a single diffractive structure, that is with a rapidity gap in either the forward or backward hemispheres. The experimental situation is as yet unclear, see for example Ref. [14]. Using the same factorization hypothesis, diffractive heavy flavour production at hadron colliders was studied in Ref. [15].

In the present study we assume that the universal pomeron structure picture is valid, and use the quantitative information on diffractive parton distributions, extracted from HERA F_2^D data as in Ref. [13], to predict (single) diffractive Higgs cross sections at LHC, that is Higgs production with a large rapidity gap in one hemisphere.¹ The process is depicted in Fig. 1. This model of diffractive Higgs production was first studied in Ref. [1]. Recently, it has been suggested [2] that triggering on single or double diffractive events may provide a cleaner environment for discovering Higgs bosons produced via $qq \to H$. The argument is that gluons should be more copious in the pomeron, thus enhancing the Higgs signal relative to the background. However when assessing the usefulness of the single diffractive cross section in enhancing the Higgs signal, it is equally important to consider the corresponding single diffractive *background* processes. Naively, one might argue that since the important backgrounds originate in quark-antiquark annihilation $(q\bar{q} \rightarrow \gamma\gamma, ZZ)$ the gluon-rich pomeron may indeed enhance the signal to background ratio. However, care is needed with this argument. Higgs production probes parton distributions at a scale $Q^2 \sim M_H^2$, much larger than the typical Q^2 scales of diffractive deep inelastic scattering at HERA. Perturbative DGLAP evolution of the diffractive parton distributions to these high scales gives rise to a mixing of the quark and gluon distributions such that, for example, a large g/q ratio at small scales is washed out at higher scales. It is a priori not clear, therefore, that the signal to background ratio is enhanced in diffractive events. It is precisely this question that we wish to study here, using the three models of pomeron structure presented in Ref. [13].

In the following we shall present numerical results for single diffractive Higgs production at the future CERN LHC collider ($\sqrt{s} = 14 \text{ TeV}$) with the underlying parton distributions of the pomeron as presented in [13]. These three pomeron models are obtained from fits to HERA measurements of the diffractive structure function $F_2^D(x, Q^2; x^{\mathbb{P}}, t)$ [17, 18], and are described in detail in Ref. [13]. In the present context, the most important distinguishing feature of the models is the gluon distribution in the pomeron, which differs significantly between them. In summary:

Model 1: At $Q_0 = 2$ GeV the pomeron is entirely composed of quarks. Gluons are dynamically generated via DGLAP evolution.

Model 2: A mix of quarks and gluons at the starting scale Q_0 .

¹The cross sections for double diffractive production, with two rapidity gaps, are readily estimated in this approach by combining two sets of diffractive parton distributions. Numerically, these are found to be much smaller. For other approaches to double diffractive Higgs production see Ref. [16].

Model 3: A predominantly hard gluonic content at the starting scale, the gluons in the pomeron carry large fractional momenta on average.

The Q^2 evolution of the gluon distributions $\xi f_{g/\mathbb{P}}(\xi, Q^2)$, with $\xi = x/x^{\mathbb{P}}$, for the three models is shown in Fig. 2. The quark distributions are comparable for all three models, being constrained by the HERA data, which explains why the cross sections for diffractive W^{\pm} and Z production (via $q\bar{q} \to W, Z$) are rather similar in the three models [13], in contrast to the Higgs cross sections to be presented below.

The dominant mechanism for Higgs production at the LHC is gluon–gluon fusion via a top quark loop, see for example Ref. [19].² The leading–order cross section is given by [20]

$$\frac{d\sigma}{dy_H}(pp \to HX) = \sigma_0 I\left(\frac{m_t^2}{M_H^2}\right) f_{g/p}(x_1, Q^2) f_{g/p}(x_2, Q^2), \tag{2}$$

with

$$\sigma_0 = \frac{G_F \alpha_S^2(Q^2)}{32\sqrt{2\pi}} \frac{M_H^2}{s},$$
(3)

for a Higgs boson of mass M_H and rapidity y_H . The function I in (2) can be approximated by

$$I(x) \approx 1 + \frac{1}{4x}, \qquad \text{for } x > 1.$$
(4)

The longitudinal momentum fractions of the gluons inside the colliding protons are $x_{1,2} = (M_H/\sqrt{s})e^{\pm y_H}$. The single diffractive Higgs cross section is obtained from (2) by replacing one of the $f_{g/p}$ by the corresponding diffractive parton distribution, i.e.

$$\frac{d\sigma^{SD}}{dy_H}(pp \to HX) = \sigma_0 I\left(\frac{m_t^2}{M_H^2}\right) \left[f_{g/p}^D(x_1, Q^2) f_{g/p}(x_2, Q^2) + f_{g/p}(x_1, Q^2) f_{g/p}^D(x_2, Q^2)\right],$$
(5)

where

$$f_{g/p}^D(x,\mu^2) = \int dx^{\mathbb{P}} dt \ \frac{df_{g/p}(x,\mu^2;x^{\mathbb{P}},t)}{dx^{\mathbb{P}} dt},\tag{6}$$

with $df_{g/p}/dx^{\mathbb{P}}dt$ given by Eq. (1). In the calculations which follow, the integration ranges are taken to be

$$0 \le x^{\mathbb{P}} \le 0.1, \qquad 0 \le -t < \infty. \tag{7}$$

For the parton distributions $f_{i/p}(x, Q^2)$ in the proton we use the MRS(A') set of partons [21], with QCD scale parameter $\Lambda_{\overline{MS}}^{N_f=4} = 231$ MeV, which corresponds to $\alpha_S(M_Z^2) = 0.113$. At the level of accuracy to which we are working, all modern parton distribution sets give essentially the same results. The renormalization/factorization scale is chosen to be

²In our calculations we also include the direct $q\bar{q} \rightarrow H$ (q = u, d, c, s, b) quark–fusion processes, but these are numerically much less important.

 $Q^2 = M_H^2$. We use leading-order expressions for the signal and background cross sections, since our primary interest is in the *ratio* of diffractive to total cross sections, which should not be significantly affected by higher-order corrections to the basic subprocesses. In any case, the diffractive parton distribution fits to the deep inelastic data do not yet require NLO corrections.

The cleanest decay channel for searching for the intermediate mass Higgs boson at the LHC is $H \to \gamma\gamma$, with $\operatorname{Br}(\operatorname{H} \to \gamma\gamma) \sim 3 \times 10^{-4} - 3 \times 10^{-3}$ for 50 GeV $\leq M_H \leq 150$ GeV [19]. The irreducible background comes from the $O(\alpha^2) q\bar{q} \to \gamma\gamma$ and the $O(\alpha^2 \alpha_s^2) gg \to \gamma\gamma$ [22] subprocesses. Note that these provide *lower* bounds to the background cross sections, since reducible backgrounds from e.g. $qg \to \gamma q(q \to \gamma, \pi^0, \ldots)$ can also be important in practice, see for example Ref. [23]. In what follows we will ignore these additional contributions, assuming that they can be suppressed by photon isolation cuts. For larger Higgs masses, i.e. for $M_H > 2M_Z$, the important decay channel is $H \to ZZ \to 4l^{\pm}$, with $\operatorname{Br}(\operatorname{H} \to \operatorname{ZZ}) \approx 0.3$ [19]. In this range, the dominant irreducible background is from $q\bar{q} \to ZZ$.

In Fig. 3a we show the total (2) and single diffractive (5) Higgs cross sections, the latter calculated using the three sets of pomeron parton distributions of Ref. [13]. As expected, Model 3 with the largest gluon gives the largest diffractive cross section. Model 1 has no gluons at all at the starting scale $Q_0 = 2$ GeV; gluons are dynamically created via DGLAP evolution at higher values of Q. However, the gluon distribution remains quite small compared to Models 2 and 3. Taking the models together, we see that between approximately 2% and 15% of Higgs events are expected to be singly diffractive.³ Our results for the single diffractive and total Higgs cross sections are consistent with those obtained in Ref. [2] using similar models.

Fig. 3b shows the $\gamma\gamma$ background for the lower part of the mass range, with M_H now replaced by the $\gamma\gamma$ invariant mass $M_{\gamma\gamma}$. Note that in *both* Figs. 3a and 3b we impose a cut of $|y_{\gamma}| \leq 2$ to approximately account for the experimental acceptance. As the inset in Fig. 3b shows, the gluon-gluon fusion process dominates for very small $M_{\gamma\gamma}$ where small parton momentum fractions are probed. The $q\bar{q}$ subprocess dominates at large $M_{\gamma\gamma}$. The corresponding single diffractive cross sections are again largest for the gluon-richer pomeron models, in particular Model 3. However, even the gluon-poor Model 1 becomes comparable to Model 2 due to the increasing $q\bar{q}$ contribution to the cross section at large $M_{\gamma\gamma}$.

The ZZ backgrounds, relevant for higher Higgs masses, are shown in Fig. 4b. We see that in contrast to the $\gamma\gamma$ backgrounds of Fig. 3b, all three pomeron models give comparable diffractive cross sections over the entire M_{ZZ} range. This is because the diffractive quark distributions are constrained to be the same by the HERA F_2^D data.

Before discussing the single diffractive ratios of the signal and background processes,

³Recall that we impose a cut $x^{\mathbb{P}} \leq 0.1$ when calculating the diffractive cross sections.

it is interesting to study in more detail the kinematics of diffractive Higgs production, in particular the typical values of the various momentum fractions in the calculation. Thus in Fig. 5 we show the average gluon momentum fraction $\langle x \rangle$ inside the pomeron, the momentum fraction $x^{\mathbb{P}}$ of the pomeron and the average value of the variable ξ with $\langle \xi \rangle = \langle x/x^{\mathbb{P}} \rangle$, as a function of M_H . The calculation of these quantities allows the Higgs cross sections in the different models to be related to the parton distributions of Fig. 2. The gluon momentum fraction shows the typical $\langle x \rangle \propto M_H/\sqrt{s}$ behaviour which follows from the input $x_{1,2} = (M_H/\sqrt{s})e^{\pm y_H}$ for the momentum fractions of the gluons in $gg \to H$, Eq. (2). The fractional pomeron momentum is of course constrained to be $x^{\mathbb{P}} \leq 0.1$ and it stays very close to this upper limit throughout the complete range of M_H . It exhibits an almost linear but very weak M_H dependence for $M_H \ge 100$ GeV: $\langle x^{\mathbb{P}} \rangle \sim 3.2 \times 10^{-5} M_H$. The relevant variable for comparison with the parton distributions in Fig. 2 is $\xi = x/x^{\mathbb{P}}$. For light Higgs masses the values for $\langle \xi \rangle$ are small, ($\langle \xi \rangle < 0.1$ for $M_H < 100$ GeV). In this region of $Q = M_H$ Models 2 and 3 (cf. Figs. 2b and 2c) have approximately the same gluon content, which explains the similarity of the corresponding diffractive cross sections in Fig. 3a. For higher values of M_H , the difference between Model 2 and Model 3 becomes more apparent: the gluon distribution in Model 3 remains roughly constant, while that of Model 2 decreases for higher values of M_H and ξ . This explains the differences between Models 2 and 3 in Figs. 3a and 4a. We assume that the kinematics illustrated in Fig. 5 for the Higgs cross sections are also valid for the $\gamma\gamma$ and ZZ backgrounds at the equivalent invariant mass.

Finally we present the single diffractive ratios $R^{SD} = \sigma^{SD}/\sigma$ for the signal $(pp \rightarrow H + X)$ and background contributions $(pp \rightarrow \gamma\gamma + X, pp \rightarrow ZZ + X)$ to see whether the signal to background ratio is indeed enhanced by the gluon-rich pomeron. Fig. 6a shows the ratios for the Higgs mass range $M_H \leq 200$ GeV. For the gluon-rich Models 2 or 3, there is indeed a slight enhancement of R^{SD} for the signal compared to the background, for example in Model 3 for a Higgs mass of $M_H = 100$ GeV we find $R^{SD}_H \sim 14\%$ compared to $R^{SD}_{\gamma\gamma} \sim 11\%$. The enhancement persists over the whole Higgs mass range. For the gluon-poor Model 1, where the gluons are dynamically produced by DGLAP evolution, the background ratio is larger than the signal ratio for $M_H > 70$ GeV. This small enhancement has to be contrasted with the (at least) factor of 5 loss in the overall production rate.

The situation becomes even more dramatic if we go to higher Higgs masses (200 GeV $\leq M_H \leq 1000$ GeV) as shown in Fig. 6b. In this case the important background to Higgs production is direct ZZ pair production via quark–antiquark annihilation, as discussed above. As expected, in Model 1 the background ratio exceeds the signal ratio by a large factor (≈ 6 for $M_H = 200$ GeV). Even the gluon–richer Model 2 yields a higher background contribution for $M_H < 350$ GeV. Only at higher masses (i.e. evolution scales) are enough additional gluons produced to enhance the signal. Only the very gluon–rich Model 3, with enough gluons even at low scales, allows for a dominant signal ratio throughout the entire mass range.

In conclusion, we have calculated single diffractive Higgs cross sections for the LHC using diffractive parton distributions based on quark and gluon constituents of the pomeron, fitted to HERA F_2^D data. In particular, we have considered three models which differ in the relative amounts of quarks and gluons. If the pomeron is gluon-rich, then between 5% and 15% (depending on the Higgs mass) of Higgs events should have a single diffractive structure. Assuming the overall validity of this 'universal pomeron structure' model, more precise measurements of F_2^D at HERA will allow more accurate predictions. However we have also shown that there is no significant enhancement of the signal to background ratio in such diffractive events. DGLAP evolution to high scales $Q \sim M_H$ automatically generates a mixture of diffractive quark and gluon distributions, and so the background processes $q\bar{q}, gg \to \gamma\gamma$ and $q\bar{q} \to ZZ$ also have a large diffractive component. It is not clear, therefore, that there is any advantage in searching for Higgs bosons at the LHC in events with rapidity gaps.

Acknowledgements

We thank Dirk Graudenz for useful discussions. This work was also supported in part by the EU Programme Human Capital and Mobility, Network 'Physics at High Energy Colliders', contract CHRX-CT93-0357 (DG 12 COMA). MH gratefully acknowledges financial support in the form of a DAAD-Doktorandenstipendium (HSP III).

References

- [1] A. Schäfer, O. Nachtmann and R. Schöpf, *Phys. Lett.* **B249** (1990) 331.
- [2] D. Graudenz and G. Veneziano, *Phys. Lett.* **B365** (1996) 302.
- [3] ZEUS collaboration: M. Derrick et al., *Phys. Lett.* B315 (1993) 481; B332 (1994) 228; B338 (1994) 483.
 H1 collaboration: T. Ahmed et al., *Nucl. Phys.* B429 (1994) 477.
- [4] P.V. Landshoff, Cambridge preprint DAMTP 96/48 (1996) [hep-ph/9605383].
- [5] G. Ingelman and P. Schlein, *Phys. Lett.* **B152** (1985) 256.
- [6] UA8 collaboration: R. Bonino et al., *Phys. Lett.* B211 (1988) 239; A. Brandt et al., *Phys. Lett.* B297 (1992) 417.
- [7] H1 collaboration: P.R. Newman, presented at the Workshop on Deep Inelastic Scattering and Related Phenomena (DIS96), Rome, April 1996.

- [8] ZEUS collaboration: H. Kowalski and E. Barberis, presented at the Workshop on Deep Inelastic Scattering and Related Phenomena (DIS96), Rome, April 1996.
- [9] K. Golec-Biernat and J. Kwiecinski, INP Cracow preprint 1734/PH (1996) [hep-ph/9607399].
- [10] A. Donnachie and P.V. Landshoff, *Phys. Lett.* **B191** (1987) 309; **B198** (1987) 590(E).
- [11] J.C. Collins, L. Frankfurt and M. Strikman, *Phys. Lett.* B307 (1993) 161.
 A. Berera and D.E. Soper, *Phys. Rev.* D50 (1994) 4328; D53 (1996) 6162.
 A. Berera, preprint PSU/TH/169 (1996) [hep-ph/9606448].
- [12] P. Bruni and G. Ingelman, *Phys. Lett.* **B311** (1993) 317.
- [13] Z. Kunszt and W.J. Stirling, University of Durham preprint DTP/96/74 (1996), to be published in Proc. Workshop on Deep Inelastic Scattering and Related Phenomena (DIS96), Rome, April 1996 [hep-ph/9609245].
- [14] CDF collaboration: presented by K. Goulianos at the 10th Topical Workshop on Proton-Antiproton Collider Physics, Batavia IL, May 1995, preprint FERMILAB-CONF-95-244-E (1995).
- [15] M. Heyssler, Z. Phys. C73 (1997) 299.
- [16] J.D. Bjorken, Phys. Rev. D47 (1993) 101.
 A. Bialas and P.V. Landshoff, Phys. Lett. B256 (1991) 540.
 J.-R. Cudell and O.F. Hernandez, Nucl. Phys. B471 (1996) 471.
 H.J. Lu and J. Milana, Phys. Rev. D51 (1995) 6107.
 V.A. Khoze, A.D. Martin and M.G. Ryskin, Durham preprint DTP/97/12 (1997) [hep-ph/9701419].
- [17] H1 collaboration: T. Ahmed et al., *Phys. Lett.* **B348** (1995) 681.
- [18] ZEUS collaboration: M. Derrick et al., Z. Phys. C68 (1995) 569.
- [19] Z. Kunszt, S. Moretti and W.J. Stirling, University of Durham preprint DTP/96/100 (1996) [hep-ph/9611397].
- [20] H.M. Georgi, S.L. Glashow, M.E. Machacek and D.V. Nanopoulos, Phys. Rev. Lett. 40 (1978) 629.
- [21] A.D. Martin, R.G. Roberts and W.J. Stirling, Phys. Lett. **B354** (1995) 155.

- [22] B.L. Combridge, Nucl. Phys. B174 (1980) 243.
 A. Carimalo, M. Crozon, P. Kessler and J. Parisi, Phys. Lett. B98 (1981) 105.
 E.L. Berger, E. Braaten and R.D. Field, Nucl. Phys. B239 (1984) 52.
- [23] Z. Kunszt and W.J. Stirling, in Proceedings of the ECFA Large Hadron Collider Workshop, Aachen, Germany, 1990, edited by G. Jarlskog and D. Rein (CERN Report No. 90–10, Geneva, Switzerland, 1989), Vol. II, p. 428.

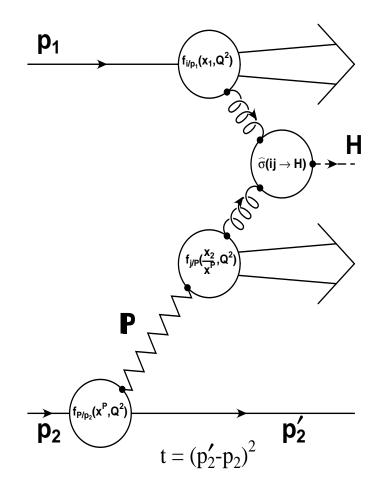


Figure 1: Kinematics of a single diffractive hard scattering event for two colliding protons, with p_2 being quasi-elastically scattered by emitting a pomeron \mathbb{P} which undergoes interaction with p_1 to create, for example, a Higgs boson H.

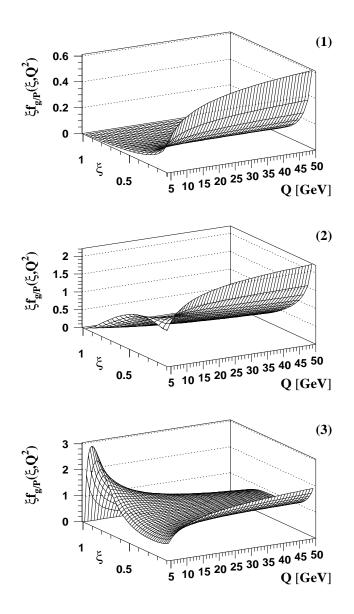


Figure 2: The Q^2 evolution of the gluon distributions $\xi f_{g/\mathbb{P}}(\xi, Q^2)$ in the three different pomeron structure models of Ref. [13].

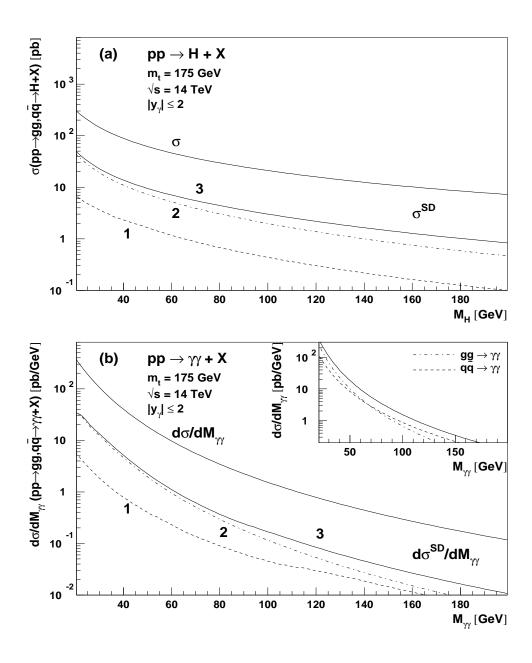


Figure 3: The total and the single diffractive cross sections for (a) Higgs production as a function of the Higgs mass M_H and (b) $\gamma\gamma$ production as a function of the invariant photon-photon mass $M_{\gamma\gamma}$ for the three different pomeron models of Ref. [13]. For both signal (assuming the decay $H \to \gamma\gamma$) and background the photons are restricted to the central region by a cut $|y_{\gamma}| \leq 2$. The inset in (b) shows the leading order cross section and the relative contributions from gluon-gluon fusion and quark-antiquark annihilation.

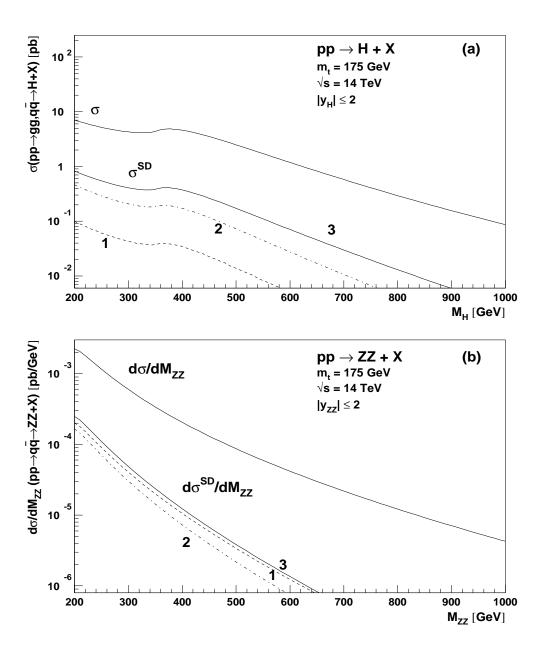


Figure 4: The total and the single diffractive cross sections for (a) Higgs production as a function of the Higgs mass M_H and (b) ZZ production as a function of the invariant ZZ mass M_{ZZ} for the three different pomeron models of Ref. [13]. The Higgs and the ZZ pair are restricted to the central region by cuts $|y_{ZZ}|, |y_H| \leq 2$.

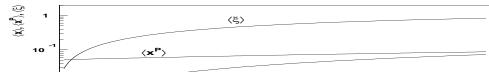


Figure 5: The average gluon fractional momentum $\langle x \rangle$, the average longitudinal momentum fraction of the pomeron $\langle x^{\mathbb{P}} \rangle$ and the average $[A]_{H \to X}$ the variable for the pomeron partor distributions $\langle \xi \rangle = \langle t / x^{\mathbb{P}} \rangle$ for different values of M_{H} in the process $pp \to H + X$.

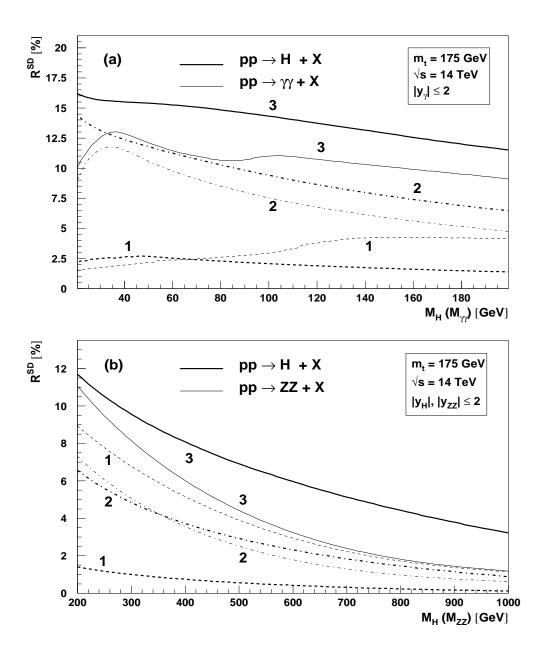


Figure 6: The single diffractive ratios $R^{SD} = \sigma^{SD}/\sigma$ for $pp \to H + X$ (solid lines) and the background contributions (a) $pp \to \gamma\gamma + X$ and (b) $pp \to ZZ + X$ (dashed lines) for the three different pomeron models. The absolute values of the cross sections σ and σ^{SD} are presented in Figs. 3 and 4.